Model Predictive Direct Speed Control With Novel Cost Function for SMPMSM Drives

Liguo Yang, Hongmei Li, *Member, IEEE*, Jiandong Huang, Zheng Zhang, and Haonan Zhao

***Abstract*—The model predictive direct speed control (MPDSC) can improve the speed dynamic performance effectively. However, due to the large difference between the mechanical and electrical time constants, short prediction could result in large current ripples at steady state, which becomes a critical problem. Besides, the conventional MPDSC methods have not deeply investigated the online-adjustable weighting factor design and the problem of i_d transient oscillation. In this article, a model predictive direct speed control with novel cost function is proposed. In the proposed method, two different q-axis current references are generated, one to improve the speed dynamics, and the other to ensure the low current ripples. The two current tracking are assigned with different weighting factors unified in one cost function. In order to determine which current tracking to play a major role under different operations, the speed error is designed as weighting factor. With the proposed cost function and designed weighting factor, the high speed dynamics and low steady current ripples can be achieved simultaneously. Finally, the effectiveness of proposed method is verified by experiments.**

***Index Terms*—High speed dynamics, low steady current ripples, model predictive direct speed control (MPDSC), novel cost function design, weighting factor.**

I. Introduction

PERMANENT magnet synchronous motor (PMSM) has been widely used in various industrial applications due to its high power density and high efficiency. Recently, the finite-control set model predictive control (FCS-MPC) becomes one of the most promising control techniques for PMSM drive system under the rapid development of microprocessors. Compared with the traditional controllers, the major advantages of FCS-MPC is that it can take advantage of the inherent discrete nature of power converters and consider different control objectives, nonlinearities and constraints in a very flexible manner [1]–[3].

The most popular FCS-MPC strategies in PMSM drives include predictive current control (PCC) and predictive torque control (PTC) [4]–[9]. However, most of PCC or PTC strategies are only applied for the current or torque control loops, and a proportional–integral (PI) regulator is normally required for the outer speed loop. In order to ensure the stability and noise immunity, the bandwidth of PI regulator is always restricted to a relative low level. Therefore, even the inner MPC controller slightly improves the speed dynamics, the transient response of speed is still unsatisfactory [10]. However, in the various industrial applications, such as the steel mill drive, annealing line, and the servo control, the transient speed performance is always crucial for the productivity of the process and quality of the product [11].

To improve the speed dynamics, the model predictive direct speed control is proposed in recent years [10], [12]–[18]. Unlike the conventional methods, the MPDSC eliminate the cascade structure and use a single predefined cost function to control the speed and current directly. Because of the characteristic of "direct control," the MPDSC exhibit fast transient response and excellent disturbance rejection performance.

However, due to the large difference between mechanical and electrical time constants, MPDSC requires long prediction horizon to include both speed and current dynamics [15]. When the MPDSC controller adopts short prediction horizon, the large current ripples at steady state could be a critical issue [13], [16]. The solution to this problem can be divided into two categories. The first solution achieves direct speed control by using long the prediction horizon. In [12], a three-step prediction MPDSC is used, and the maximum torque per ampere (MPTA) and flux weakening trajectory is added into the cost function. However, even the prediction horizon is extended, the current ripples are still relatively large. In [13], the myopic prediction is recognized as the major cause of large torque ripples; therefore, the errors of speed and flux in $(k+3)$ and $(k+4)$ instant are considered to suppress the torque oscillation. The second solution uses short prediction, but incorporates additional control variables into cost function to deal with this challenge. A novel MPDSC method is developed in [14] and [15] in which the switching states that generate high frequencies component in the stator currents are penalized, therefore, smooth current waveform can be obtained. In [16], the cost function take into account both speed and current error in which the current error is considered as an indirect control to improve the steady performance, while the speed error is recognized as a direct control to keep fast speed dynamics. With the consideration of current dynamics, the q-axis current ripples are suppressed effectively. In [17] and [18], the cost function includes the speed error and torque error; thus, low

Manuscript received August 27, 2021; revised November 12, 2021 and January 9, 2022; accepted February 18, 2022. Date of publication March 1, 2022; date of current version April 28, 2022. This work was supported in part by the National Natural Science Foundation of China under Grant 51877064 and in part by the Anhui Provincial Key Research and Development Program Funding under Grant 1804a09020092. Recommended for publication by Associate Editor A. M. Trzynadlowski. *(Corresponding author: Hongmei Li.)*

The authors are with the School of Electrical Engineering and Automation, Hefei University of Technology, Hefei 230009, China (e-mail: liguo.yang@mail.hfut.edu.cn; hongmei.li@hfut.edu.cn; jiandong.huang@mail.hfut.edu.cn; hfutzhangzheng@mail.hfut.edu.cn; hfutzhaohaonan@mail.hfut.edu.cn).

Color versions of one or more figures in this article are available at https://doi.org/10.1109/TPEL.2022.3155465.

Digital Object Identifier 10.1109/TPEL.2022.3155465

steady torque ripples can be ensured. Moreover, in [10], instead of controlling the speed and torque independently, the speed error and torque error are combined into a new sliding manifold term in the cost function, and desired speed and torque tracking are realized. The above-mentioned schemes effectively suppress the steady current ripples and achieve high speed dynamics under the framework of MPDSC. However, there still are some problems to be solved.

First, there are few reports on weighting factor design in MPDSC. For the cost function of MPC methods, weighting factors play an essential role in balancing the different nature of multiple control objectives. However, the tuning of weighting factor is always a challenging issue, which is usually determined in empirical or heuristic ways. The normalization is a widely used technique to eliminate the difference of unit and magnitude of system variables [19]. Moreover, some researches adopt ranking-based methods [20] to avoid the weighting factors, but this method limits the secondary objectives severely. Besides, there are some online adjustable tuning methods, such as neural network [21], fuzzy method [22], or stepwise changed method [23]. Compared to the offline ways, the online tuning is preferable due to the improved operation-adaptability. However, these mentioned methods are relatively complicated and have not been applied in MPDSC. In fact, there are few reports on the online weighting factor design in MPDSC, and most of the MPDSC methods take a fixed tradeoff during operations. Therefore, the conventional MPDSC methods are difficult to optimize their performance under different operating conditions.

Moreover, in the conventional MPDSC methods, the variables in *d*-axis and *q*-axis cannot be equally controlled in the acceleration transients. During acceleration operations, the speed tracking error would be much larger than i_d current tracking error. This significant speed error attracts nearly all the control weight in the cost function. Under this condition, the current in the *d*-axis exhibits obvious fluctuation. The oscillating i_d in turn deteriorate the acceleration performance. In [24], to avoid to exacerbate this problem with two-norm, the one-norm cost function is used to mitigate this phenomenon, and the i_d oscillation is reduced. In [25], additional transient cost function part is introduced in which the torque tracking and i_d control is weighted equally. During the accelerations, the transient cost function part play a major role in the whole cost function and the large i_d oscillation is suppressed. Unfortunately, this problem has been only mentioned in few methods. The deep investigation is still required, and the cost functions need to be reorganized in a more reasonable way.

In this article, the conventional MPDSC methods are reviewed, and a novel cost function is developed. First, brief analysis about weighting design and i_{d} transient oscillation are implemented. Then, a novel separated design for transients and steady state is proposed. In order to simplify the cost function design, the original speed error is converted into an equivalent transient current error. Besides, to suppress the steady current ripples, additional current reference is generated based on the PI regulation. In other words, there are two *q*-axis current references with different characteristics to be generated, one is transient reference to improve speed dynamics and the other is steady reference to ensure low steady current ripples. These two *q*-axis current tracking are assigned with different weighting factor unified in one cost function. In order to determine which current tracking to play a major role according to the operating conditions, the speed error is designed as a weighting factor instead of tracking error in the conventional manner. With the designed cost function and weighting factor, high speed dynamics and low current ripples can be achieved simultaneously under different operations.

II. Mathematical Model of PMSM Drive System

The continuous-time mathematical model of surface mounted PMSM (SMPMSM) in the synchronous *d–q* frame is written as

$$\begin{cases} \frac{di_d}{dt} = \frac{1}{L_d}\ (u_d - R_s i_d + \omega_e L_q\, i_q) + f_d \\ \frac{di_q}{dt} = \frac{1}{L_q}\,(u_q - R_s i_q - \omega_e L_d i_d - \omega_e \psi_f) + f_q \\ \frac{d\omega_m}{dt} = \frac{1}{J}\ \left(\frac{3}{2}\, p\, \psi_f\, i_q - T_L\right) + f_\omega \end{cases} \tag{1}$$

where u_{d}, u_q, i_d, and i_q denote the *dq*-axes stator voltages and currents. R_{s} is the stator resistance. L_d and L_q are the *dq*-axes inductances. ψ_f is the rotor flux linkage established by the permanent magnets. ω_m and ω_e are the mechanical and electrical angular speed. J is the moment of inertia; p is the number of pole pairs; T_{L} is the load torque. The $f_{\mathrm{d}}, f_{\mathrm{q}}$, and f_ω represent the uncertainties and external disturbance caused by the variation of motor parameters, magnetic saturation, etc.

In order to get rid of the dependence of motor parameters, the ultra-local model of PMSM is used to predict the speed and current in this article. The application of ultra-local model in the PMSM drives has already reported and validated [26], [27]. The main idea of ultra-local model is to update the motor model continually by using the data of input and output of a moving window. The ultra-local model of PMSM drives is written as

$$\begin{cases} \frac{di_d}{dt} = F_d + \alpha_d u_d \\ \frac{di_q}{dt} = F_q + \alpha_q u_q \\ \frac{d\omega_m}{dt} = F_\omega + \alpha_\omega i_q \end{cases} \tag{2}$$

where F_d, F_q, and F_ω represent the lumped uncertainties and unknown disturbance in the electrical and mechanical systems respectively. α_d, α_q, and α_ω represent the coefficients of *dq*-axes voltages to current and *q*-axis current related to torque.

Compared with (1), F_d and F_q include the resistance voltage drops, the back electromotive force, the unmolded dynamics, and uncertainties, F_ω contains the load torque, friction torque and unknown disturbance, and they can be expressed as

$$\begin{cases} F_{\mathrm{d}} = -\frac{R_{\mathrm{s}}}{L_d} i_d + \frac{L_q}{L_d}\omega_e i_q + (\frac{1}{L_d} - \alpha_d)\, u_d + f_d \\ F_q = -\frac{R_{\mathrm{s}}}{L_q} i_q - \frac{1}{L_q}(\omega_e L_d i_d + \psi_f) + (\frac{1}{L_q} - \alpha_d)\, u_q + f_q \\ F_\omega = (-\alpha_\omega i_q + \frac{3p\psi_f}{2J} i_q) - \frac{1}{J} T_L + + f_\omega. \end{cases} \tag{3}$$

The next crucial step is to estimate the F_d, F_q, and F_ω by using the information of input and output in a moving window.

This process can be realized with the algebraic parameter identification techniques [26] and the results can be written as

$$\begin{cases} \hat{F}_d = -\frac{3!}{T_F^3}\int_0^{T_F}\left((T_F-2\delta)\ i_d(\delta)+\alpha_d\,\delta\,(T_F-\delta)\,u_d(\delta)\right)d\delta \\ \hat{F}_q = -\frac{3!}{T_F^3}\int_0^{T_F}\left((T_F-2\delta)\ i_q(\delta)+\alpha_q\,\delta\,(T_F-\delta)\,u_q(\delta)\right)d\delta \\ \hat{F}_\omega = -\frac{3!}{T_F^3}\int_0^{T_F}\left((T_F-2\delta)\ \omega_m(\delta)+\alpha_\omega\,\delta\,(T_F-\delta)\,i_q(\delta)\right)d\delta. \end{cases} \tag{4}$$

Based on the discretization of (2), the discrete ultra-local prediction model can be expressed as

$$\begin{cases} i_d(k+1) = \left(\hat{F}_d(k)+\alpha_d\,u_d(k)\right)T_s + i_d(k) \\ i_q(k+1) = \left(\hat{F}_q(k)+\alpha_q\,u_q(k)\right)T_s + i_q(k) \\ \omega_m(k+1) = \left(\hat{F}_\omega(k)+\alpha_\omega\,i_q(k)\right)T_s + \omega_m(k). \end{cases} \tag{5}$$

In the MPDSC method, additional load observer is required to predict the speed in the future instant. However, from (3), it can be seen the total load information is contained in the F_ω when the ultra-local model is used as prediction model.

III. Conventional MPDSC Methods

In this section, the conventional cost function design is reviewed briefly in Section III-A. Then, the limitation of the conventional MPDSC methods is analyzed in Section III-B and Section III-C.

A. Conventional Cost Function Design

The MPDSC methods predict the speed and current in discrete steps and select the optimal voltage vector according to the cost function. The speed error minimization is the main objective and the secondary objective is the MTPA trajectory tracking. The cost function can design as

$$J_1 = \lambda_\omega(\omega_m^* - \omega_m^p)^2 + \lambda_d(i_d^* - i_d^p)^2 + C_{\lim} \tag{6}$$

where the i_d^* is always set to zero for SMPMSM drive system, λ_ω and λ_d are the weighting factors for each term. $C_{\lim}$ is used to prevent the current from exceeding the maximum value

$$C_{\lim} = \begin{cases} 0 & i_d^2 + i_q^2 \le I_{\max}^2 \\ \infty & i_d^2 + i_q^2 > I_{\max}^2 \end{cases} \tag{7}$$

where $I_{\max}$ is the maximum accessible current.

However, the cost function J_1 requires a long prediction horizon due to the large difference between mechanical time constant and electrical one. When J_1 with short prediction horizon is used, large current ripples will exist at the steady state. Due to the different "time scale characteristic," the current changes swiftly with the voltage variation, but the speed acts relative slowly to the current variation. Therefore, the speed is further insensitive to the voltage variation. When the "one–step"prediction horizon is utilized, a very aggressive voltage vector will be chosen to achieve minimum speed error at (k+2) instant. However, due to the different sensitiveness of speed and current to voltage, the chosen voltage vector that enable the minimum speed error, may result in much high-frequency component in stator currents, in other words, large current ripples. This problem can be addressed by using long prediction horizons but that will cause a high computation burden to microprocessors.

To realize high speed dynamics and reduce the steady current ripple with a short prediction horizon, additional intermediate control variables are added in the cost function J_1. These cost functions are summarized as follows:

$$\begin{cases} J_2 = \lambda_\omega(\omega_m^* - \omega_m^p)^2 + \lambda_d(i_d^* - i_d^p)^2 + \lambda_q(i_q^* - i_q^p)^2 + C_{\lim} \\ J_3 = \lambda_\omega(\omega_m^* - \omega_m^p)^2 + \lambda_d(i_d^* - i_d^p)^2 + \lambda_q(i_q^{pf})^2 + C_{\lim} \\ J_4 = \lambda_\omega(\omega_m^* - \omega_m^p)^2 + \lambda_d(i_d^* - i_d^p)^2 + \lambda_T(T_e^p - T_l)^2 + C_{\lim} \\ J_5 = |S| + \lambda_d(i_d^* - i_d^p)^2 + \lambda_\omega(\omega_m^* - \omega_m^p)^2 + C_{\lim} \end{cases} \tag{8}$$

where i_d^* is the q-axis current reference generated by a linear controller; i_q^{pf} is high-pass filtered version of the q-axis current, the variable S is a sliding manifold term of $c\ (\omega_m^* - \omega_m^p) + (T_e^p - T_l)$. Although these cost functions [10], [14]–[18] present in different forms, their design principle is similar. During the transient state, the speed error is large, thus the voltage vector selection mainly depends on the speed error, which ensures to achieve excellent speed dynamics. During the steady state, the speed error is extremely low, and the consideration of the intermediate variable errors is dedicated to suppressing the high-frequency components in the stator currents. By introducing the new intermediate variables, the cost function can well incorporate the speed and current dynamics, and the one-step prediction MPDSC becomes feasible.

B. Weighting Factor

For the conventional MPDSC methods, a relatively large weighting factor is assigned to speed error to achieve precise speed control and high dynamics. This large control weight is helpful to achieve really extraordinary performance of speed tracking. However, due to the large difference between mechanical and electrical time constants, this high speed dynamics is achieved at the sacrifice of large current ripples. Actually, there is a tradeoff between performance of speed tracking and rejection of high-frequency component in steady-stator currents. The really better way is to keep dominant control weight in speed tracking during the transients and increase the control weight of torque or current control at the steady state. However, the weighting factors are always fixed values in the conventional methods, in which large weight of speed error will increase the steady current ripples, while a small one will compromise the speed dynamic performance. In other words, these two contradictory goals cannot be well balanced in different operations with fixed weighting factors.

C. Unequal Control in D-Axis and Q-Axis

Another problem of the conventional MPDSC is the tracking errors in d-axis and q-axis are not penalized equally. During the acceleration transients, the speed tracking term attract almost all the control weight in the cost function, and the i_d oscillates under these operations, which in turn deteriorates the acceleration performance. This problem comes from two reasons. The first reason lies the small weighting factor in the i_d tracking term. To

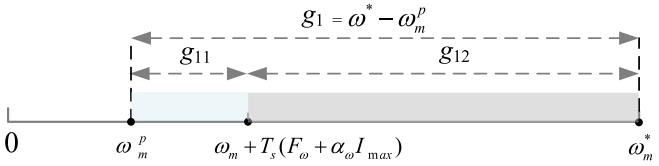

Fig. 1. Decomposition of speed errors.

obtain the fast speed dynamics, the weighting factor of speed error λ_ω is always much larger than that of d-axis current λ_d, which may be reasonable in the steady state, but intensifies the i_d oscillation in the acceleration transients. The other reason is the conventional speed error does not consider the current constraint and invalid speed error part is incorporated.

The speed error g_1 can be divided into two parts: g_{11} and g_{12}, as shown in Fig. 1. Due to the current safety constraints, the maximum speed that motor can be reached in one control period is the value of $\omega_{\rm m}+T_{\rm s}(F_\omega+\alpha_\omega I_{\rm max})$. Therefore, only the g_{11} is valid speed error, which plays a positive role to select the optimal voltage vector. While the error g_{12} is a constant during a control period, which has no contribution for the voltage vector selection. But, the error g_{12} account a great proportion in the cost function during the accelerations, which attracts the most of control weight concentrating on the speed tracking. Therefore, the speed error g_{12} is an irrational speed error part which should not get any weight in the cost function. Based on the analysis, a simple and effective method is proposed in the following section to avoid the i_d oscillation from the perspective of weighting factor and cost function design.

IV. Proposed MPDSC Method

In order to keep high speed dynamics in transients and low current ripples at steady state, this article proposes a novel cost function. Two different q-axis current references are generated, one called transient reference to keep fast speed dynamics and the other called steady reference to ensure low current ripples. Moreover, the speed error is designed as a weighting factor, and it is used to determine which current tracking to play a major role according to the operating conditions. The designed cost function shown as

$$J = \lambda_t C_t + \lambda_s C_s + (\lambda_s + \lambda_t)\, C_d + C_{\rm lim} \tag{9}$$

where C_t is $(i_{qt}^* - i_q^p(k+2)^2)$, C_s is $(i_{qs}^* - i_q^p(k+2)^2)$, and C_d is $(i_d^* - i_d^p(k+2)^2)$, λ_s is a fixed weighting factor, λ_t is the speed error $(\omega_m^* - \omega_m(k))^2$ and i_{qt}^*, i_{qs}^* denote the transient q-axis current reference and steady q-axis current reference. The schematic diagram of proposed MPDSC shown as Fig. 2 .

A. Generation of Transient Q-Axis Current Reference

In order to simplify the design of cost function, the original speed error is converted into equivalent transient current error C_t and the transient q-axis current reference i_{qt}^* is derived based on the inverse mechanical model in (5). Due to the solution equivalence, the transient current error C_t is equivalent to the

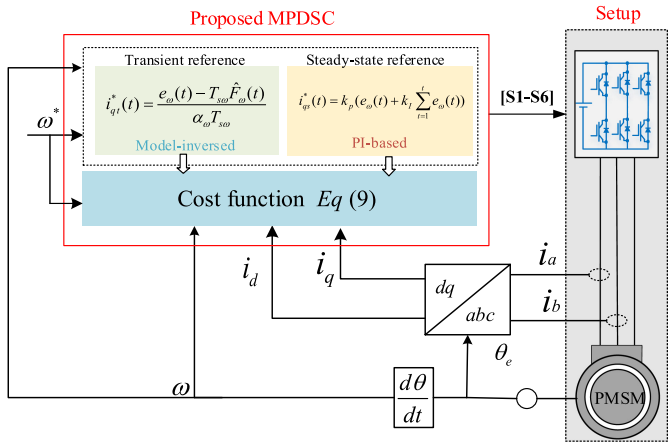

Fig. 2. Schematic diagram of the proposed MFPDSC.

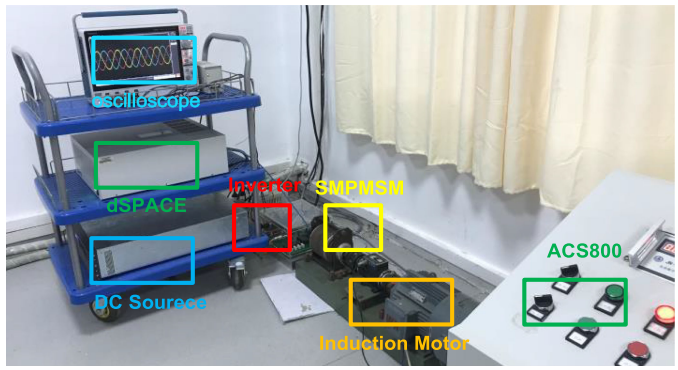

Fig. 3. Laboratory bench.

original speed error g_{11}

$$i_{qt}^*(t) = \frac{\omega_m^*(t+1) - \omega_m(t) - T_{s\omega}\hat{F}_\omega(t)}{\alpha_\omega T_{s\omega}} \tag{10}$$

$$i_{qt}^*(t) = \begin{cases} i_{qt}^*(t) & i_{qt}^*(t) \le I_{\rm max} \\ I_{\rm max} & i_{qt}^*(t) > I_{\rm max} \end{cases} \tag{11}$$

where $T_{s\omega}$ denotes the update period for i_{qt}^*, and $T_{s\omega}$ is ten times of current sampling period T_s, so the term "t " and "k" are used to represent different periods.

By using i_{qt}^*, the characteristic of "direct speed control" is well maintained, and good speed dynamics can be achieved. More importantly, it is intuitive to consider the current limit in C_t with (11), which is equivalent to eliminate the g_{12} in the conventional cost functions.

B. Generation of Steady Q-Axis Current Reference

The i_{qt}^* well keeps the characteristic of "direct speed control," and superior speed dynamics can be obtained. However, the i_{qt}^* is generated by short prediction, and the large current ripples at steady state could become a problem. In order to improve the steady current control performance, another steady q-axis current reference i_{qs}^* is then generated based on PI regulation

and shown as

$$i_{qs}^{*}(t) = k_p \left(e_\omega(t) + k_i \sum_{t=1}^{t} e_\omega(t) \right) \tag{12}$$

$$i_{qs}^{*}(t) = \begin{cases} i_{qs}^{*}(t) & i_{qs}^{*}(t) \leq I_{\max} \\ I_{\max} & i_{qs}^{*}(t) > I_{\max} \end{cases} \tag{13}$$

where $e_\omega(t)$ denote the speed error at the instant t, k_p, and k_i are the proportional and integral gains.

There are some benefits to introduce i_{qs}^{*} based on the PI regulation. First, the i_{qs}^{*} is fundamental to zero-offset speed tracking. Moreover, due to the presence of integrator the negative impact of quantization noise under high sampling frequency is lowered. By introducing the i_{qs}^{*}, the drawback of "direct speed control" is compensated effectively, and smooth current is offered.

C. Weighting Factors

Unlike the fixed weighting factor design of conventional MPDSC methods, the proposed weighting factors consist of a variable one and fixed ones. The speed error is used to be a variable weighting factor λ_t for transient current error C_t, and it is updated with the operations in real time. Besides, a fixed weighting λ_s is assigned to steady current error C_s. In order to penalize d-axis and q-axis current errors equally, the sum of λ_s and λ_t set as the weighting factor for C_d. This means the variables in d and q axis are equally controlled in an intrinsic way and the i_d transient oscillation is effectively avoided.

As all the control objectives in (9) are in current form, there is of great convenience to the tuning of weight factor, and the λ_s can be selected according to the value of maximum steady speed ripples. Compared with the conventional MPDSC methods, trial and error tuning way is avoided. Moreover, the speed error as a variable weighting factor is online updated by which a better tradeoff is achieved.

D. Explanation of the Cost Function

The proposed cost function develops a separate design for transients and steady state, which can combine the merit of direct speed control and PI regulator under the framework of FCS-MPC. During the transients, the λ_t is much larger than λ_s, so the C_t and C_d plays a decisive role in voltage vector selection. At the steady state, the speed error is extremely low and the λ_t is smaller than λ_s, thus, the voltage selection mainly depends on the C_s and C_d. In other words, the proposed cost function plans different tracking behaviors for transient and steady state. The variable weighting factor λ_t is used to activate the optimized tracking according to the operation conditions. Moreover, because the speed error is converged to zero continuously, the q-axis current can be very smoothly transit between i_{qt}^{*} and i_{qs}^{*}. By using the proposed cost function, the high speed dynamics and low current ripples can be achieved simultaneously. The difficulty in the tradeoff between speed performance and rejection of high-frequency component in currents can be well solved with the separated design manner.

TABLE I
PARAMETERS OF TESTED SMPMSM

Name	Symbol	Value
Rated Power	P_n	900/W
Rated Torque	T_n	13/ N·m
Stator Resistance	R_s	0.957/ Ω
Stator inductance	L_s	1.0/ mH
PM flux linkage	ψ_f	0.027/ Wb
Pole Pairs	p	12
Moment of inertia	J	0.01015/kg·m^2
DC link Voltage	V_{dc}	48 /V

E. Delay Compensation

In the real-time implementation, the microprocessor needs some time to compute the iterations. There will be a delay between the instant at which the currents are measured and application of the new switching state [28]. In the proposed method, the one-step delay compensation is considered, in which the (k+2) instant errors instead of (k+1) instant errors are minimized. The previous optimal vector is used to estimate the current value at (k+1) instant.

V. EXPERIMENTAL RESEARCH

A comparative research with another three control methods is implemented. The first control method is PI-based speed control in cascade structure: the outer speed loop uses the PI regulator and the inner current loop uses the FCS current predictive controller. The second control method is PSC1 which is the conventional method with cost function of J_1 in (6). The third comparative scheme is PSC2 whose cost function is J_4 in (8).

The laboratory bench consists of 0.9 kW SMPMSM as controlled motor and 2.2 kW induction motor as load. The SMPMSM is driven by a two level power inverter, and motor parameters are given in Table I. The load motor is driven by ABB ACS800 to provide controllable load torque. The algorithms execute on dSPACE DS1007 real-time platform with control desk and MATLAB/Simulink. The laboratory bench is shown as Fig. 3.

The sampling time of three control methods is 50 μs. To ensure fairness of comparisons, all the methods use the ultra-local model expressed by (5) as prediction model. The $\alpha_{d,}$ and α_q is given the value of $1/L_s$, and α_ω is given the value as $1.5p\psi_f/J$. Besides, the length of moving window should be less than the electrical time constant. Therefore, the window length $n_F T_s$ can be normally selected as 5 to 20 times that of the control period, and n_F selected as 10 in this article. More details of the parameter selection relevant to the model-free system are discussed in [23] and [24].

In the PI speed control scheme, the PI regulator is equipped with clamping antiwindup technique. The proportional and integral gains are designed as: $k_p = J\omega_{sc}/1.5p\psi_f$ and $k_i = \omega_{sc}/5$, where the ω_{sc} is the bandwidth of speed loop [29], and it is selected as 239 rad/s. Moreover, the designed PI parameters are

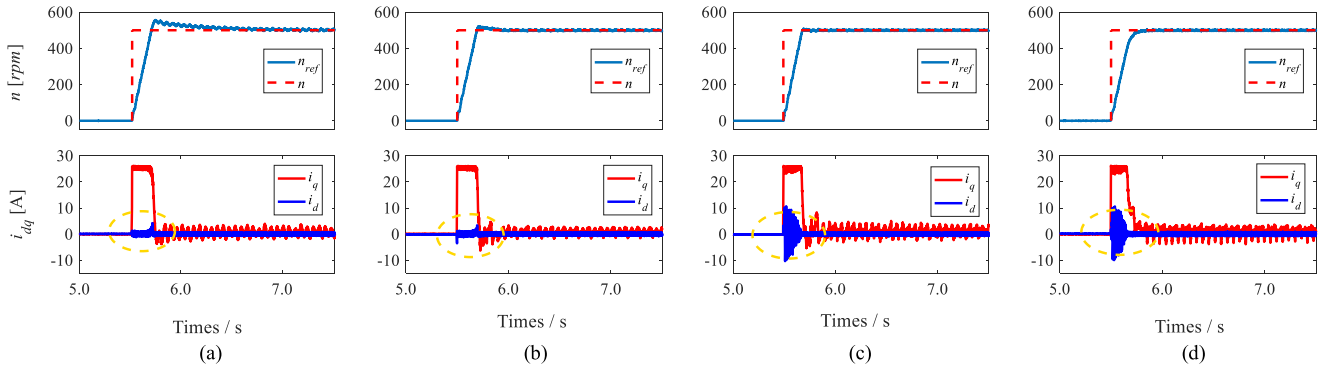

Fig. 4. 500 r/min startup without load. (a) PI based. (b) Proposed MPDSC. (c) PSC1. (d) PSC2.

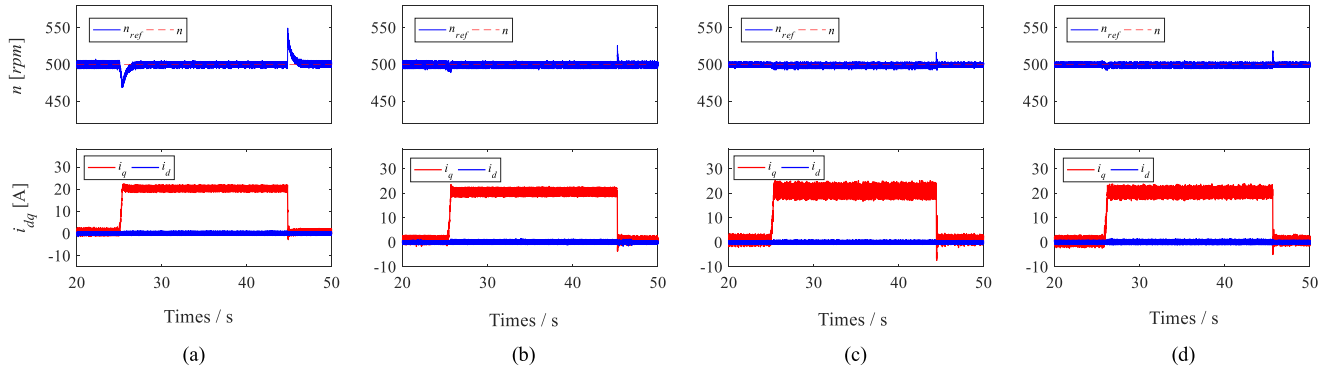

Fig. 5. 10 N·m step load at 500 r/min. (a) PI based. (b) Proposed MPDSC. (c) PSC1. (d) PSC2.

further optimized by the experiments and selected as $k_p = 5, k_i = 0.01$ finally. In the proposed method. the PI parameters are tuned by the same method in the first scheme and selected as $k_p = 5$, $k_i = 0.05$. In this experimental bench, the value of maximum speed ripples is about 5 r/min; therefore, λ_s is selected as 1.0 and the influence of its value on system performance is discussed later. In method PSC1, the λ_ω and λ_d are tuned as 150 and 0.1, respectively. In the method PSC2, the λ_ω, λ_d, and λ_T are tuned from the experiments as 150, 0.10, and 0.40, respectively.

TABLE II
TRANSIENT PERFORMANCE OF 500 R/MIN WITH 10 N·M STEP-LOAD

Parameters/Method	PI	Proposed	PSC1	PSC2
Positive step load settling time/s	1.33	0.38	0.05	0.20
Negative step load settling time/s	1.28	0.15	0.11	0.12
Positive step load variation/r/min	30.20	10.80	3.50	6.60
Negative step load variation /r/min	49.40	25.50	16.50	17.5

A. Dynamic Performance

1) Startup Without Load: The experimental results of 500 r/min startup operations shown in Fig. 4. Among the four methods, the PSC1 has the small speed overshoot 8.4 r/min and the PI scheme has the largest speed overshoot of 55 r/min. The PSC2 does not have any overshoot. For the proposed MPDSC, its cost function still maintains the PI characteristics partially. The proposed method has the speed overshoot of 21.9 r/min. From the perspective of settling times, the method PSC1 and PSC2 have similar small settling time of 0.26 and 0.32 s, the PI scheme has the largest settling time of 1.43 s, and the settling time of the proposed method is 0.32 s. The conventional MPDSC methods PSC1and PSC2 have excellent startup performance due to its "direct speed control" property. However, due to the inherent contradiction between rapidity and overshoot of PI regulator, the PI scheme has limited dynamic performance. For the proposed method, during the startup, the C_t plays a decisive role in the cost function; thus, the "direct speed control" characteristic is well maintained, and fast startup can be achieved, which is close to the conventional MPDSC results.

Besides, in the conventional MPDSC methods PSC1 and PSC2, the i_d transient oscillation is not suppressed due to the less control weight in *d*-axis during the acceleration operations. While this phenomenon is well avoided in the proposed control method. It indicates that the proposed cost function realizes equal controls in both the *d*- and *q*-axis intrinsically.

2) Step-Load Transients: Figs. 5 and 6 show the experimental results of 500 r/min with10 N·m step load and 100 r/min with 5 N·m step load. A positive step load is applied at 25 s, and a negative step load is applied at 43 s. The specific results are given in Tables II and III. It needs to note that the induction motor

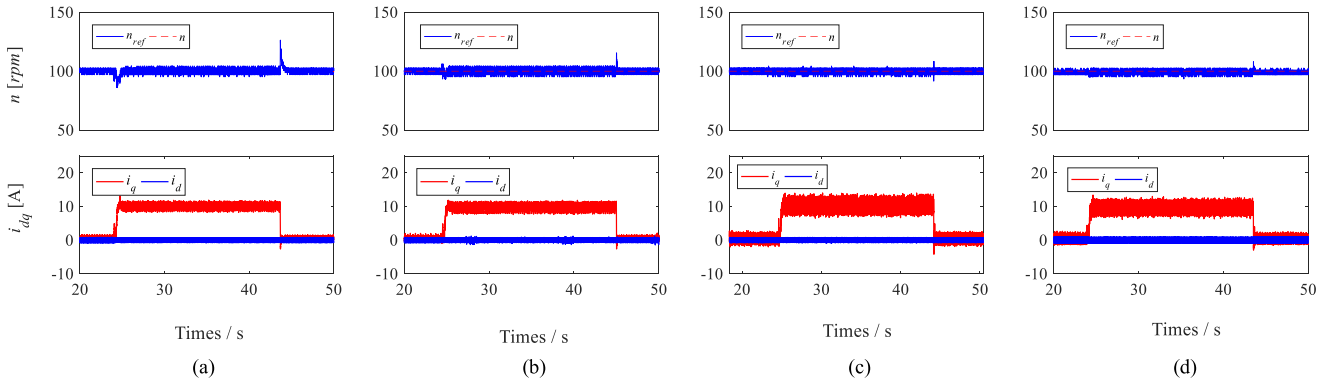

Fig. 6. 5 N·m step load at 100 r/min. (a) PI based. (b) Proposed MPDSC. (c) PSC1. (d) PSC2.

TABLE III
TRANSIENT PERFORMANCE OF 100 R/MIN WITH 5 N·M STEP LOAD

Parameters/Method	PI	Proposed	PSC1	PSC2
Positive step load settling time/s	0.97	0.43	0.08	0.10
Negative step load settling time/s	0.68	0.22	0.06	0.15
Positive step load variation /r/min	14.5	7.59	4.78	5.30
Negative step load variation /r/min	26.00	15.40	8.00	8.80

TABLE IV
STEADY PERFORMANCE OF 500 r/min WITH 10 N·M

Parameters/Method	PI	Proposed	PSC1	PSC2
Steady speed ripples /r/min	± 4.8	± 4.8	± 4.6	± 4.6
Steady i_d ripples /A	2.10	2.15	2.12	2.12
Steady i_q ripples /A	3.48	3.73	7.52	5.23
THD / %	3.20	3.28	4.93	4.75

TABLE V
STEADY PERFORMANCE OF 100 R/MIN WITH 5 N·M

Parameters/Method	PI	Proposed	PSC1	PSC2
Steady speed ripples /r/min	±5.0	±5.0	± 4.5	± 4.5
i_d ripples /A	1.68	1.69	1.64	1.64
i_q ripples /A	3.05	3.82	6.70	5.68
THD / %	7.04	7.87	10.45	10.07

cannot produce an ideal positive step load, but the negative step can seem as an ideal step change. It is evident that the PI scheme has the largest speed changes when a step load is applied, and it requires the longest time to restore to the speed reference. The proposed MPDSC method has fast transient response, which is close to the conventional methods PSC1 and PSC2. When a step load is applied, the weighting factor λ_t becomes much larger than λ_s, and the transient tracking behavior is activated at instant. Therefore, fast speed response is obtained. It indicates that the proposed weighting factor can effectively identify the operation conditions and activate the appropriate tracking.

B. Steady-State Performance

The steady-state performance of 500 r/min with 10 N·m and 100 r/min with 5 N·m is given in Tables IV and V. The waveforms and total harmonic distortion (THD) results are displayed from Figs. 7 to 12, respectively. From the perspective of speed ripples, the four methods all track the speed reference precisely, and their speed performances at steady state are almost the same. However, from the perspective of the current ripples, the method PSC1 has the largest q-axis current ripples and worst THD among four methods, while the current ripples of PI scheme are much lower. It indicates that although the PI scheme has a limited transient response, its current performance at steady state is much better than that of the "direct speed control." For the method PSC2, the current ripples are suppressed due to the consideration of torque tracking in the cost function compared to the PCS1. For the proposed MPDSC, during the steady operations, the C_s and C_d play a decisive role in the cost function because the speed error is extremely low at that time. Thus, the proposed MPDSC can present very close performance with the PI method at the steady state. In a word, the proposed MPDC can well combine the merits of PI scheme and "direct speed control." Therefore, the high speed dynamics and low current ripples can be achieved simultaneously.

Moreover, it shows different noise in the q-axis current waveform of Figs 7 and 8. This reason of this phenomenon comes from two aspects. The first reason is nature of short prediction MPDSC with much high-frequency component in current. Therefore, the q-axis current in the methods PSC1 and PSC2 have relatively more noise. The other reason is different filter are employed in the speed raw signal processing. In the PI-based scheme, the first order low-pass filter is used to deal with the raw speed signals and its cut frequency is 500 Hz. In the PSC1and PSC2, in order to not compromise the high speed dynamics, only $N = 5$ mean filtering is used to slightly filter out the speed signal noise. In the proposed method, both filters are utilized: 500 Hz cut frequency low-pass filter in the generation of i_{qs}^* reference, and $N = 5$ mean filtering in the

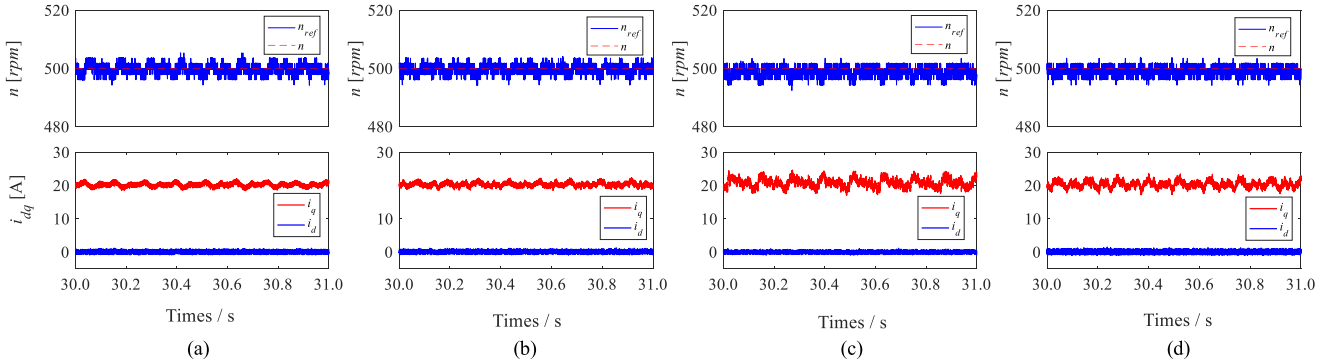

Fig. 7. Steady-state performance at 500 r/min with 10 N·m. (a) PI based. (b) Proposed MPDSC. (c) PSC1. (d) PSC2.

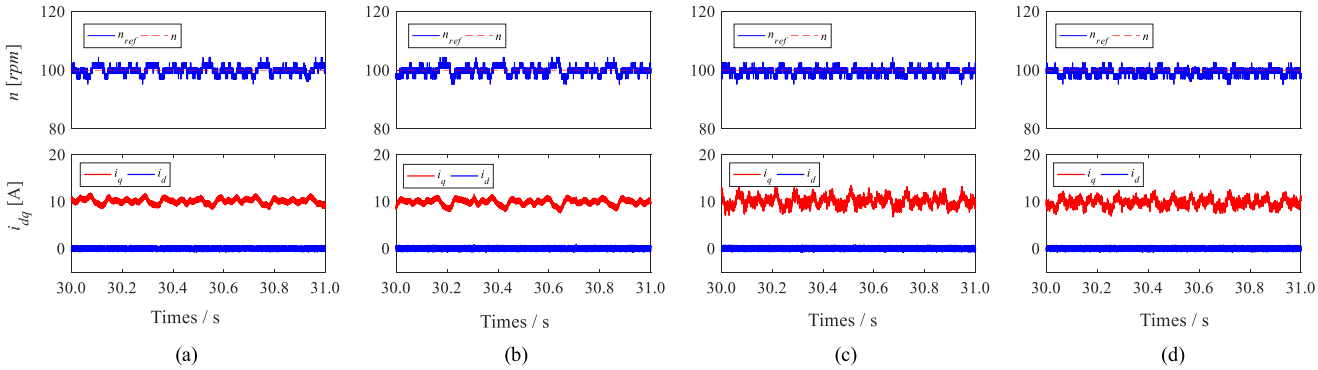

Fig. 8. Steady-state performance at 100 r/min with 5 N·m. (a) PI based. (b) Proposed MPDSC. (c) PSC1. (d) PSC2.

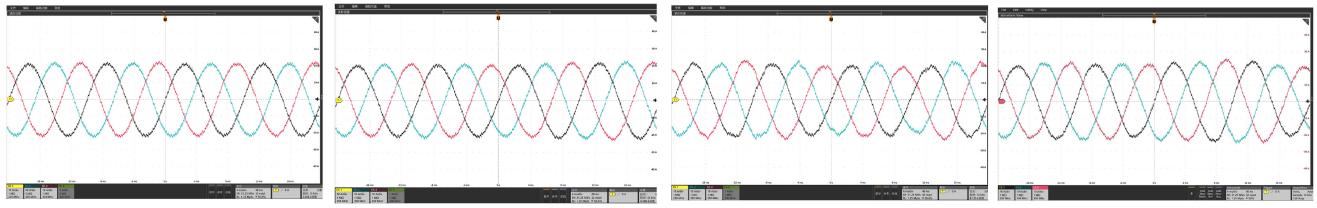

Fig. 9. Three phase current waveform at 500 r/min with 10 N·m. (a) PI based. (b) Proposed MPDSC. (c) PSC1. (d) PSC2.

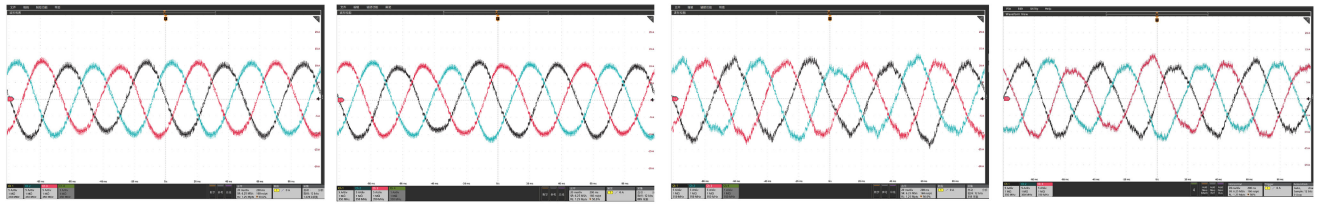

Fig. 10. Three phase current waveform at 100 r/min with 5 N·m. (a) PI based. (b) Proposed MPDSC. (c) PSC1. (d) PSC2.

generation i_{qt}^* reference. Thanks for the separate design for transients and steady state, different filtering can be well unified. It is the distinctiveness of FCS-MPC with higher flexibility and additional degrees of freedom. From the experimental results, the embed low-pass filter is not compromise the transient speed performance and smooth stator currents can be obtained.

C. *Influence of Weighting Factor*

In order to investigate the influence of the fixed weighting factor λ_s on the performance of MPDSC, five different λ_s are tested under the same operating conditions. These test operations include 300 r/min startup without load, 300 r/min with step

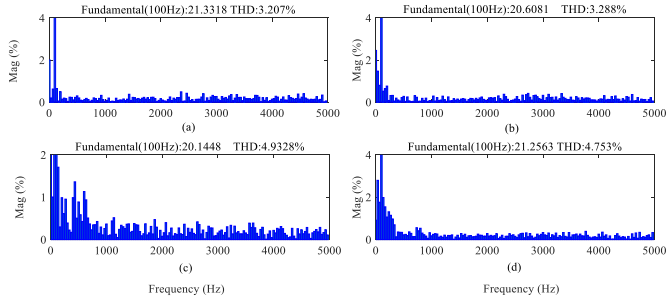

Fig. 11. THD result of A phase current at 500 r/min with 10 N·m. (a) PI method. (b) Proposed MPDSC. (c) PSC1. (d) PSC2.

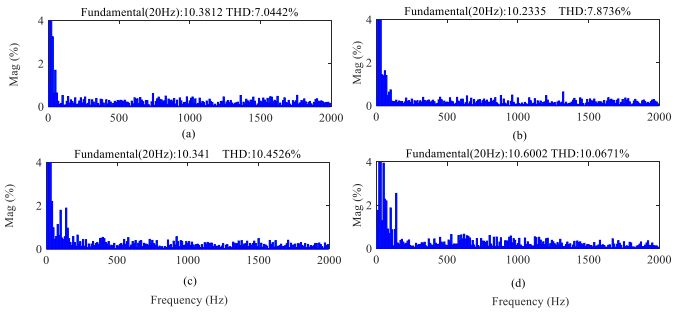

Fig. 12. THD result of A phase current at 100 r/min with 5 N·m. (a) PI method. (b) Proposed MPDSC. (c) PSC1. (d) PSC2.

TABLE VI
300 R/MIN WITH DIFFERENT WEIGHING FACTORS

Parameters/ λ_s value	0.3	0.5	1	2	5
Steady speed ripples /r/min	± 4.4	± 4.6	± 4.3	± 4.5	± 4.1
Steady i_{d} ripples /A	1.82	1.76	1.74	1.80	1.82
Steady i_{q} ripples /A	3.20	3.15	2.88	2.90	2.91
Positive step load undershoot /r/min	8.70	8.80	8.80	8.80	8.70
Negative step load overshoot/r/min	22.4	24.1	25.8	29.5	31.4
Start-up settling time/s	0.30	0.31	0.33	0.32	0.33
Positive step settling time/s	0.37	0.39	0.41	0.45	0.46
Negative step load settling time/s	0.16	0.17	0.17	0.21	0.27

change load from 0 to 10 N·m and 10 to 0 N·m. The experimental results are given in Table VI. It indicates that a large λ_s could degrade the ability of load disturbance rejection, and the fast speed dynamics is compromised. On the contrary, a small λ_s could improve the speed dynamic, but the steady-state current ripples will be increased. In other words, the tuning of λ_s also need to tradeoff between high speed dynamics and low current ripples. However, the experimental results suggest the performance is not deteriorated drastically even the λ_s varies in a wide range. Thus, the sensitivity of the controller to weighting factor is greatly reduced for the proposed MPDSC.

VI. CONCLUSION

A MPDSC method with a novel cost function is proposed for SMPMSM drive system in this article. The proposed method develops a separate design for the transient and steady state by introducing the different q-axis current references. The speed error plays a role of weighting factor instead of the tracking error as the traditional manner. Therefore, the proposed method well combines the merit of "direct speed control" and PI regulation under the framework of FCS-MPC. Due to the flexibility, it can keep low current ripples at steady state and maintain high speed dynamics during the transients. Compared with the conventional MPDSC, methods, the subtle contribution of this article can be summarized as follows.

1) *Better Tradeoff Between the Performance of Transients and Steady State:* In the conventional MPDSC methods, the speed dynamics and current ripples are two contradictory goals and difficult to be balanced with fixed weighting factors. In the proposed method, a better tradeoff is achieved with the separated design.
2) *Simplified Weighting Factor Tuning:* In the proposed method, the tracking objectives are all converted into the current form, and the weighting factor tuning is really simplified. Only λ_s needs to be tuned and its value can be computed easily. While two at least weighting factor need to be tuned and their tuning is much challenging in conventional methods.
3) *Equal control in the* d- *and* q-*axis:* The proposed method can penalize the tracking error in d- and q-axis equally through the modification of cost function and weighting factor design. The i_d transient oscillation problem is avoided intrinsically.

REFERENCES

[1] S. Kouro, P. Cortes, R. Vargas, U. Ammann, and J. Rodriguez, "Model predictive control—A simple and powerful method to control power converters," *IEEE Trans. Ind. Electron.*, vol. 56, no. 6, pp. 1826–1838, Nov. 2009.
[2] S. Vazquez, J. Rodriguez, M. Rivera, L. G. Franquelo, and M. Norambuena, "Model predictive control for power converters and drives: Advances and trends," *IEEE Trans. Ind. Electron.*, vol. 64, no. 2, pp. 935–947, Nov. 2017.
[3] J. Rodriguez *et al.*, "State of the art of finite control set model predictive control in power electronics," *IEEE Trans. Ind. Informat.*, vol. 9, no. 2, pp. 1003–1016, Oct. 2013.
[4] J. Rodriguez, R. M. Kennel, J. R. Espinoza, M. Trincado, C. A. Silva, and C. A. Rojas, "High-performance control strategies for electrical drives: An experimental assessment," *IEEE Trans. Ind. Electron.*, vol. 59, no. 2, pp. 812–820, Jun. 2012.
[5] Y. Zhang, D. Xu, J. Liu, S. Gao, and W. Xu, "Performance improvement of model-predictive current control of permanent magnet synchronous motor drives," *IEEE Trans.Ind. Appl.*, vol. 53, no. 4, pp. 3683–3695, Apr. 2017.
[6] Z. Zhou, C. Xia, Y. Yan, Z. Wang, and T. Shi, "Torque ripple minimization of predictive torque control for PMSM with extended control set," *IEEE Trans. Ind. Electron.*, vol. 64, no. 9, pp. 6930–6939, Mar. 2017.
[7] Y. Zhang and H. Yang, "Two-vector-based model predictive torque control without weighting factors for induction motor drives," *IEEE Trans. Power Electron.*, vol. 31, no. 2, pp. 1381–1390, Mar. 2016.
[8] Y. Wang *et al.*, "Deadbeat model-predictive torque control with discrete space-vector modulation for PMSM drives," *IEEE Trans. Ind. Electron.*, vol. 64, no. 5, pp. 3537–3547, Jan. 2017.
[9] Y. Zhou, H. Li, R. Liu, and J. Mao, "Continuous voltage vector model-free predictive current control of surface mounted permanent magnet synchronous motor," *IEEE Trans. Energy Convers.*, vol. 34, no. 2, pp. 899–908, Aug. 2019.

[10] X. Gao, M. Abdelrahem, C. M. Hackl, Z. Zhang, and R. Kennel, "Direct predictive speed control with a sliding manifold term for PMSM drives," *IEEE J. Emerg. Sel. Topics Power Electron.*, vol. 8, no. 2, pp. 1258–1267, Jun. 2020.

[11] S.-K. Sul, *Control of Electric Machine Drive Systems*. Hoboken: NJ, USA: Wiley, 2011.

[12] M. Preindl and S. Bolognani, "Model predictive direct speed control with finite control set of PMSM drive systems," *IEEE Trans. Power Electron.*, vol. 28, no. 2, pp. 1007–1015, Jun. 2013.

[13] M. Liu, K. W. Chan, J. Hu, W. Xu, and J. Rodriguez, "Model predictive direct speed control with torque oscillation reduction for PMSM drives," *IEEE Trans. Ind. Informat.*, vol. 15, no. 9, pp. 4944–4956, Feb. 2019.

[14] E. J. Fuentes, C. Silva, D. E. Quevedo, and E. I. Silva, "Predictive speed control of a synchronous permanent magnet motor," in *Proc. IEEE 6th Int. Power Electron. Motion Control Conf.*, Feb. 2009, pp. 390–395.

[15] E. J. Fuentes, C. A. Silva, and J. I. Yuz, "Predictive speed control of a two-mass system driven by a permanent magnet synchronous motor," *IEEE Trans. Ind. Electron.*, vol. 59, no. 7, pp. 2840–2848, Jun. 2012.

[16] P. Kakosimos and H. Abu-Rub, "Predictive speed control with short prediction horizon for permanent magnet synchronous motor drives," *IEEE Trans. Power Electron.*, vol. 33, no. 3, pp. 2740–2750, Apr. 2018.

[17] Y. Xu, Y. Hou, and Z. Li, "Robust predictive speed control for SPMSM drives based on extended state observers," *J. Power Electron.*, vol. 19, no. 2, pp. 497–508, 2019.

[18] X. Lang, M. Yang, J. Long, Y. Li, and D. Xu, "A novel direct predictive speed and current controller for PMSM drive," in *Proc. IEEE 8th Int. Power Electron. Motion Control Conf.*, May 2016, pp. 2551–2556.

[19] C. Gong, Y. Hu, M. Ma, J. Gao, and K. Shen, "Novel analytical weighting factor tuning strategy based on state normalization and variable sensitivity balance for PMSM FCS-MPTC," *IEEE/ASME Trans. Mechatronics*, vol. 25, no. 3, pp. 1690–1694, Mar. 2020.

[20] C. A. Rojas, J. Rodriguez, F. Villarroel, J. R. Espinoza, C. A. Silva, and M. Trincado, "Predictive torque and flux control without weighting factors," *IEEE Trans. Ind. Electron.*, vol. 60, no. 2, pp. 681–690, Jul. 2013.

[21] O. Machado, P. Martin, F. J. Rodriguez, and E. J. Bueno, "A neural network-based dynamic cost function for the implementation of a predictive current controller," *IEEE Trans. Ind. Informat.*, vol. 13, no. 6, pp. 2946–2955, Apr. 2017.

[22] F. Villarroel, J. R. Espinoza, C. A. Rojas, J. Rodriguez, M. Rivera, and D. Sbarbaro, "Multiobjective switching state selector for finite-states model predictive control based on fuzzy decision making in a matrix converter," *IEEE Trans. Ind. Electron.*, vol. 60, no. 2, pp. 589–599, Jun. 2013.

[23] L. M. A. Caseiro, A. M. S. Mendes, and S. M. A. Cruz, "Dynamically weighted optimal switching vector model predictive control of power converters," *IEEE Trans. Ind. Electron.*, vol. 66, no. 2, pp. 1235–1245, Apr. 2019.

[24] X. Liu *et al.*, "Continuous control set predictive speed control of SPMSM drives with short prediction horizon," *IEEE Trans. Power Electron.*, doi: 10.1109/TPEL.2021.3118270.

[25] H. Abu-Rub, M. Malinowski, and K. Al-Haddad, *Model Predictive Speed Control of Electrical Machines in Power Electronics for Renewable Energy Systems, Transportation and Industrial Applications*. Hoboken, NJ, USA: Wiley, 2014.

[26] Y. Zhou, H. Li, and H. Zhang, "Model-free deadbeat predictive current control of a surface-mounted permanent magnet synchronous motor drive system," *J. Power Electron.*, vol. 18, no. 1, pp. 103–115, 2018.

[27] Y. Zhou, H. Li, H. Zhang, J. Mao, and J. Huang, "Model free deadbeat predictive speed control of surface-mounted permanent magnet synchronous motor drive system," *J. Elect. Eng. Technol.*, vol. 14, no. 1, pp. 265–274, 2019.

[28] J. Rodriguez and P. Cortes, *Predictive Control of Power Converters and Electrical Drives*. Hoboken, NJ, USA: Wiley, 2012.

[29] K. H. Nam, *AC Motor Control and Electrical Vehicle Applications*. Boca Raton, FL, USA: CRC Press, 2019.

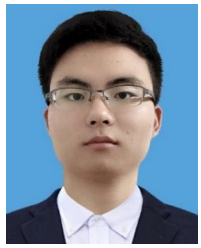

Liguo Yang was born in Shanxi, China, in 1996. He received the B.S. degree from the Shenyang University of Technology, Shenyang, China, in 2018. He is currently working toward Ph.D. degree with the Department of Electrical Engineering and Automation, Hefei University of Technology, Hefei, China.

His research interests include control of permanent magnet synchronous motors.

Hongmei Li (Member, IEEE) was born in Anhui, China, in 1969. She received the B.S. and M.S. degrees from the Hefei University of Technology, Hefei, China, in 1991 and 1996, respectively, and the Ph.D. degree from the Shenyang University of Technology, Shenyang, China, in 2003, all in electrical engineering.

Since 2006, she has been a Professor with the Department of Electrical Engineering, Hefei University of Technology, Hefei, China. From 2004 to 2005, she was a Visiting Scholar with Hikihara Laboratory, Kyoto University, Kyoto, Japan. In 2012, she joined as a Visiting Scholar with the Center for Automotive Research, The Ohio State University, Columbus, OH, USA. Her research interests include the design and control of permanent magnet machines, power electronics, fault diagnosis, and fault-tolerant control of electrical machine systems.

Jiandong Huang was born in Anhui, China. He received the B.S. degree in electronic information engineering from Hefei University, Hefei, China, in 2017. He is currently working toward the Ph.D. degree with the Department of Electrical Engineering and Automation, Hefei University of Technology, Hefei, China.

His research interests include the control of electrical motor drives.

Zheng Zhang was born in Anhui, China, in 1995. He received the B.S. degree in electrical engineering from Jiamusi University, Heilongjiang, China, in 2017. He is currently working toward the Ph.D. degree with the Department of Electrical Engineering and Automation, Hefei University of Technology, Hefei, China.

His research interests include predictive control of electrical machine systems.

Haonan Zhao was born in Anhui, China, in 1998. He received the B.S. degree from Anhui Jianzhu University, Hefei, China, in 2020.He is currently working toward the Ph.D. degree with the Department of Electrical Engineering and Automation, Hefei University of Technology, Hefei, China.

His research interests include the model-free control of electrical motor drives.